The Cryosphere Discuss., 7, 2801–2843, 2013
www.the-cryosphere-discuss.net/7/2801/2013/
doi:10.5194/tcd-7-2801-2013
© Author(s) 2013. CC Attribution 3.0 License.

The Cryosphere Discussions
Open Access

This discussion paper is/has been under review for the journal The Cryosphere (TC).
Please refer to the corresponding final paper in TC if available.

Grain shape influence on light extinction in snow

Q. Libois[1], G. Picard[1], J. L. France[2], L. Arnaud[1], M. Dumont[3], C. M. Carmagnola[3], and M. D. King[2]

[1]UJF – Grenoble 1/CNRS, Laboratoire de Glaciologie et Géophysique de l'Environnement (LGGE) UMR 5183, Grenoble, 38041, France
[2]Department of Earth Sciences, Royal Holloway University of London, Egham, Surrey, TW20 0EX, UK
[3]Météo-France – CNRS, CNRM – GAME UMR 3589, Centre d'Etudes de la Neige, Grenoble, France

Received: 16 May 2013 – Accepted: 20 May 2013 – Published: 17 June 2013

Correspondence to: Q. Libois (quentin.libois@lgge.obs.ujf-grenoble.fr)

Published by Copernicus Publications on behalf of the European Geosciences Union.

Abstract

The energy budget and the photochemistry of a snowpack greatly depend on the penetration of solar radiation into the snowpack. While representing snow by a collection of spherical particles has been a successful option in the numerical computation of the albedo, such models poorly reproduce light extinction measurements. Here, we explore the limits of the spherical representation by using numerical tools and experimental data. For this, we investigate the influence of grain shape on light extinction in the visible and near-infrared (NIR) ranges. To compute light extinction, we developed a multi-layer radiative transfer model based on the δ-Eddington approximation and analytical expressions of the albedo, α, and the asymptotic flux extinction coefficient (AFEC), k_e. The snowpack is characterized by the profiles of density, specific surface area (SSA) and two parameters (B and g^G) depending only on the grain shape. The aim of the paper is to estimate the values of B and g^G and to understand how they impact macroscopic optical properties of snow. First, the values of B and g^G are deduced from simulations with ray tracing models for a variety of simple geometric shapes. The results show that spherical grains propagate light deeper into snow than the other shapes we have investigated, in agreement with theoretical and experimental studies from the literature. Then we present an experimental method to retrieve B for natural snow using optical measurements. Analytical expressions of albedo and AFEC demonstrate that B can be retrieved from simultaneous measurements of albedo and AFEC of a snow layer, or similarly from vertical profiles of reflectance and light intensity in a snowpack. Such measurements were performed in Antarctica and in the Alps and led to values of B between 0.8 and 2.0, which significantly differs from the theoretical value for spherical grains: $B = 1.25$. In addition, values of B were estimated from data in the literature. This led to a wider range of values (1.0–9.9) which may be partially explained by the accuracy of the data. We demonstrate that grain shape has a significant influence on AFEC in natural snow. It highlights the large variety of natural snow microstructure and the importance of considering grain shape for snow optics questions. It experimentally

TCD
7, 2801–2843, 2013

demonstrates that spherical grains are inappropriate to model light extinction in snow, an important result that should be considered in further studies dedicated to subsurface absorption of shortwave radiation and snow photochemistry.

1 Introduction

Snow is involved in strong feedback loops in the climate system (Cess et al., 1991; Hall, 2004) because its optical properties depend on some snow physical characteristics (grain size, density, impurities) that themselves evolve with atmospheric conditions (Colbeck, 1982; Picard et al., 2012). Snow is highly reflective in the visible and NIR range (Warren, 1982) so that the amount of solar energy absorbed by the snowpack is small with respect to vegetation, bare soil or bare ocean for instance, but varies significantly with slight changes of snow physical properties. Snow is also semi-transparent so that the solar energy penetrates within the snowpack and is partly absorbed in depth below the surface (Colbeck, 1989). Although Brandt and Warren (1993) highlight that most of the absorption occurs in the very top centimeters of the snowpack, the penetration of light has a crucial impact on the thermal regime (Liston and Winther, 2005; Flanner, 2005; Kuipers Munneke et al., 2009; Picard et al., 2012) and on the availability of photons for photochemical reactions (King and Simpson, 2001; Domine et al., 2008). The amount, and vertical distribution, of the absorbed energy, are determined by the albedo, and the AFEC, respectively. Both quantities are highly wavelength dependent (Warren, 1982). Modeling these quantities from given snow physical properties is crucial for general circulation models (Hall and Qu, 2006; Waliser et al., 2011) and photochemistry models (e.g. Lee-Taylor and Madronich, 2002).

The computation of snow optical properties from microstructural properties (often reduced to grain size and density) has been investigated in many studies using radiative transfer theory (e.g. Chandrasekhar, 1960). According to this theory, snow is represented by a continuous medium with appropriate absorption and scattering properties. In order to calculate these quantities from the snow physical properties, that

TCD
7, 2801–2843, 2013

can be measured in the field or predicted by snow evolution models (Brun et al., 1989, 1992; Vionnet et al., 2012), it is necessary to assume that snow is composed of individual grains and that the grains have a particular shape. Spherical grains have often been used (Wiscombe and Warren, 1980; Warren, 1982; Brandt and Warren, 1993), firstly because Mie's electromagnetic calculations (Mie, 1908) provide an analytical and rigorous formulation and secondly because the albedo calculated with other grain shapes can be close to the albedo calculated with spheres if the grain size is appropriately chosen (Warren, 1982). In particular, Grenfell and Warren (1999) emphasized that any grain type can be replaced by a collection of spheres of equal specific surface area (SSA = $S/\rho_{\text{ice}}V$) as for irregular grains albedo calculations. However subsequent theoretical studies show that replacing snow grains by spheres of equal SSA is not entirely satisfying since single-scattering properties, including single-scattering albedo and asymmetry factor, are different from one shape to another (Neshyba et al., 2003; Kokhanovsky and Zege, 2004; Grenfell et al., 2005; Picard et al., 2009).

Also, the spherical assumption seems inadequate for the prediction of the bi-directional reflectance function (BRDF) of snow (Sergent et al., 1998; Aoki et al., 2000; Dumont et al., 2010), that is critical for the interpretation of remote sensing data. Negi and Kokhanovsky (2011) use fractal particles for satellite snow grain size retrieval. Zege et al. (2008) point out that for snow composed of dendritic or facetted crystals the snow grain size retrieval algorithm they use leads to errors of 50 % if spherical grains are assumed. On the contrary, the experimental study on metamorphosed snow by Gallet et al. (2009) shows that spheres are adequate to relate bi-hemispherical albedo and SSA within ±12 %. Although snow grains are not spherical, the spherical assumption remains the simplest way of representation and is largely used for meteorological and climate purposes (van den Broeke et al., 2008; Kuipers Munneke et al., 2012), as well as for photochemistry applications (Zatko et al., 2012).

Quantitative studies of light extinction in snow are scarce compared to studies of light reflection (Bohren and Barkstrom, 1974; Perovich, 2007). Performing accurate extinction measurements is difficult since the introduction of sensors perturbs the medium

TCD
7, 2801–2843, 2013

(Dunkle and Bevans, 1956; Giddings and LaChapelle, 1961) and repeat experiments demonstrate uncertainties of ∼ 20 % as a result of measurement error and natural variability of snow (France et al., 2011b; France and King, 2012). The few attempts to reproduce measurements of light extinction, using radiative transfer models with the spherical assumption, failed (Sergent et al., 1987; Meirold-Mautner and Lehning, 2004). In particular, Sergent et al. (1987) measured AFEC twice greater than those predicted by a model with spherical grains (their Fig. 6).

The objective of the present paper is to investigate the performance of the spherical assumption to compute albedo and light extinction. To this end, this work is based on an analytical formulation of the radiative transfer theory, where snow grain shape is fully defined by two parameters, the absorption enhancement parameter B and the asymmetry factor g^{G} (Kokhanovsky and Zege, 2004). In Sect. 2, we derive analytical expressions of the two measurable optical properties (albedo and AFEC) in terms of B, g^{G}, SSA, density, and optical indices. It shows that albedo and AFEC depend on grain shape in different ways. In order to quantify the impact of the grain shape on snow optical properties, ranges of variations of B and g^{G} are needed. To the authors' knowledge, these shape parameters have never been measured for natural snow. Hence the following sections are aimed at determining the values of B and g^{G} for snow by using two approaches. The first approach is numerical and uses Monte-Carlo ray tracing methods (Sect. 3) to determine the values of B and g^{G} for a set of simple geometric shapes (Macke et al., 1996; Kokhanovsky and Macke, 1997; Picard et al., 2009). The second approach is experimental and uses optical measurements in natural snow (Sect. 4). It allows the determination of B only. Section 5 discusses the values obtained from these two approaches.

TCD
7, 2801–2843, 2013

2 A Two-stream Analytical Radiative TransfEr in Snow (TARTES) model with explicit shape dependence to compute the extinction of light in snow

Diffusion of light in snow is modeled using the radiative transfer theory (Chandrasekhar, 1960). Scattering and absorbing properties of snow depend on the single-scattering properties of individual snow grains. The latter depend on grain size and shape (Kokhanovsky, 2004), as detailed in Sect. 2.1. In the field, only macroscopic optical properties of snow (albedo and AFEC) are measurable. The asymptotic analytical radiative transfer (AART) theory (Kokhanovsky and Zege, 2004) provides analytical expressions for the albedo α and the AFEC k_e of a homogeneous snow layer, as a function of snow grains single-scattering properties (Sect. 2.2). As natural snowpacks are usually stratified, we use these analytical expressions in a multi-layer model based on the δ-Eddington approximation (Joseph et al., 1976), to calculate the albedo and extinction profile of a stratified snowpack (Sect. 2.3). Natural snow is never pure, so that light absorbing impurities have to be taken into account in the model in order to interpret experimental data in the visible range (Sect. 2.4).

2.1 Single-scattering properties of pure snow

Diffusion of light in snow is often modeled using the radiative transfer theory, which assumes that snow is a continuous medium (Bohren and Barkstrom, 1974; Wiscombe and Warren, 1980). Each layer of the snowpack is characterized by the phase function, extinction coefficient σ_e and single-scattering albedo ω which are determined from snow grain size and shape, and snow density (Bohren and Barkstrom, 1974). σ_e is related to the scattering and absorption coefficients by $\sigma_e = \sigma_s + \sigma_a$ and $\omega = \sigma_s/\sigma_e$. In the Two-stream Analytical Radiative TransfEr in Snow (TARTES) model, the snow grains in a particular layer have the same size and shape and their size is much larger than the wavelength. In such a case, calculations can be performed with the geometric optics approximation. In addition, we limit our study to the spectral range 300–1350 nm where ice is weakly absorbing (Warren and Brandt, 2008), leading to $1 - \omega \ll 1$. We assume

TCD
7, 2801–2843, 2013

the snow grains are independent scatterers (Warren, 1982). Hence summarizing rules can be applied (Melnikova, 2008), leading to expressions of σ_e and σ_a as a function of the extinction and absorption cross-sections C_{ext} and C_{abs} (m^2) of individual snow grains by:

$$\sigma_e = nC_{ext} \quad (1)$$

$$\sigma_a = nC_{abs}, \quad (2)$$

where n is the grain concentration (m^{-3}) related to the volume V of an individual grain and to snow density ρ by:

$$n = \frac{\rho}{\rho_{ice} V}. \quad (3)$$

C_{ext} is twice the average projection area Σ of the grain (Zege et al., 2008):

$$C_{ext} = 2\Sigma. \quad (4)$$

Scattering occurs each time a photon reaches the grain surface while absorption is due to the photon path within the grain. C_{abs} is thus

$$C_{abs} = B\gamma V, \quad (5)$$

where $\gamma = \frac{4\pi\chi}{\lambda}$ is the ice absorption coefficient and the wavelength dependent imaginary part of the ice refractive index χ can be found in Warren and Brandt (2008). The coefficient B depends on the shape of the particle and on the difference between the real parts of the refractive indices of ice and air. B is called the "absorption enhancement parameter" (Kokhanovsky and Zege, 2004) since it quantifies the enhancement of absorption (compared to a straight trajectory through the grain) due to lengthening of the photon paths within the grain owing to multiple internal reflections. B is independent of the size of the particle. By definition of ω it follows:

$$(1 - \omega) = \frac{B\gamma V}{2\Sigma}. \quad (6)$$

TCD
7, 2801–2843, 2013

The average cosine of the phase function, called asymmetry factor, is denoted g. In TARTES, like in the AART theory, the phase function is entirely characterized by g, which is the average of the geometric diffusion term g^{G} and the diffraction term $g^{D} \simeq 1$ (Kokhanovsky and Zege, 2004):

$$g \simeq \frac{1}{2}(g^{\mathrm{G}} + 1). \tag{7}$$

g^{G} depends on the shape and real part of the ice refractive index. It is independent of the grain size, like B. In the spectral range of interest, ice is weakly absorbing and the real part of the ice refractive index is nearly constant, so that in TARTES, B and g^{G} are considered independent of the wavelength (Fig. 4 of Wiscombe and Warren (1980) shows variations of g smaller than 3 % in the spectral range 300–1350 nm).

2.2 The asymptotic analytical radiative transfer (AART) theory

The AART theory presented in Kokhanovsky (2004) assumes that the bi-hemispherical albedo α (albedo of a semi-infinite scattering medium illuminated by a diffuse source, hereafter referred as albedo) and the AFEC k_{e} are expressed in terms of g and ω for weakly absorbing wavelengths by:

$$k_{\mathrm{e}} = \sigma_{\mathrm{e}} \sqrt{3(1-\omega)(1-g)} \tag{8}$$

$$\alpha = \exp\left(-4\sqrt{\frac{1-\omega}{3(1-g)}}\right). \tag{9}$$

$\ell = k_{\mathrm{e}}^{-1}$ is the e-folding depth, i.e. the depth at which light intensity has decreased by a factor e. Similar expressions have been derived or used in former studies (Bohren and Barkstrom, 1974; Wiscombe and Warren, 1980; Brandt and Warren, 1993). With

TCD
7, 2801–2843, 2013

the formalism presented in Sect. 2.1, Eqs. (8) and (9) become:

$$k_e \simeq \frac{\rho}{\rho_{ice}}\sqrt{\frac{3B\gamma\Sigma}{V}(1-g^G)} \tag{10}$$

$$\alpha \simeq \exp\left(-4\sqrt{\frac{B\gamma V}{3\Sigma(1-g^G)}}\right). \tag{11}$$

It follows that the value B of a semi-infinite homegenous slab of snowpack can be estimated from the albedo at wavelength λ_α and the AFEC at wavelength λ_{k_e} with:

$$B \simeq -\frac{\rho_{ice}k_e(\lambda_{k_e})\ln(\alpha(\lambda_\alpha))}{4\rho\sqrt{\gamma(\lambda_{k_e})\gamma(\lambda_\alpha)}}, \tag{12}$$

where λ_{k_e} and λ_α are wavelengths in the range of validity of the theory. They can be different or equal.

SSA ($m^2\,kg^{-1}$) is the total surface area per unit mass. For convex particles, Σ is proportional to the surface area S of the grain: $S = 4\Sigma$ (Vouk, 1948; Zege et al., 2008), so that:

$$\frac{\Sigma}{V} = \frac{\rho_{ice}SSA}{4}. \tag{13}$$

Hence for convex particles, α and k_e are eventually expressed in terms of ρ, SSA, B and g^G by:

$$k_e \simeq \rho\sqrt{\frac{3B\gamma}{4\rho_{ice}}SSA(1-g^G)} \tag{14}$$

$$\alpha \simeq \exp\left(-8\sqrt{\frac{B\gamma}{3\rho_{ice}SSA(1-g^G)}}\right). \tag{15}$$

TCD
7, 2801–2843, 2013

In Eqs. (14) and (15), $(1 - g^{G})$ is multiplied by SSA, which shows that $(1 - g^{G})$ cannot be optically measured, unless an independant measure of SSA is available (e.g. Dominé et al., 2001; Flin et al., 2004).

2.3 Extension to a multi-layer snowpack using the δ-Eddington approximation

The two-stream formulation of the radiative transfer theory (Schuster, 1905) has been widely used in snow optics to describe diffusion of light in a layered plane-parallel snowpack (Dunkle and Bevans, 1956; Schlatter, 1972; Bohren and Barkstrom, 1974; Wiscombe and Warren, 1980; King and Simpson, 2001). The formulation is accurate when photons experience a large number of scattering events before escaping the snowpack or being absorbed, i.e. at weakly absorbing wavelengths. The model TARTES uses the δ-Eddington approximation (Joseph et al., 1976) to solve the two-stream radiative transfer equation. In that case, the direct flux F^{dir} and the downward ($F_n^{\downarrow}$) and upward ($F_n^{\uparrow}$) diffuse fluxes in a horizontally homogeneous layer take the form (e.g. Jiménez-Aquino and Varela, 2005):

$$F^{\mathrm{dir}}(z) = F_{\odot} e^{-\tau(z)/\mu_0} \tag{16}$$

$$F_n^{\downarrow}(z) = A_n e^{-k_{en} z} + B_n e^{k_{en} z} + G_n^{\downarrow} e^{-\tau(z)/\mu_0} \tag{17}$$

$$F_n^{\uparrow}(z) = \alpha_n A_n e^{-k_{en} z} + \frac{B_n}{\alpha_n} e^{k_{en} z} + G_n^{\uparrow} e^{-\tau(z)/\mu_0}, \tag{18}$$

where $\tau(z)$ is the scaled optical depth at depth z (Wiscombe, 1977), $F_{\odot}$ the direct incident flux and $\mu_0 = \cos\theta_0$, with θ_0 the local zenith angle. α_n and k_{en} are the albedo and AFEC of layer n if the layer were infinite. The terms proportional to $e^{-\tau(z)/\mu_0}$ in Eqs. (17) and (18) correspond to the contribution of direct light that has been scattered only once, and quickly vanish with depth (detailed expressions of $G_n^{\downarrow}$ and $G_n^{\uparrow}$ are given in Jiménez-Aquino and Varela, 2005). Equations (17) and (18) are applied to each layer of the N-layer snowpack. The continuity conditions state that the diffuse fluxes $F_n^{\downarrow}$ and

TCD
7, 2801–2843, 2013

$F_n^{\uparrow}$ be continuous at each interface at depth L_n:

$$F_n^{\downarrow}(L_n) = F_{n+1}^{\downarrow}(L_n) \tag{19}$$

$$F_n^{\uparrow}(L_n) = F_{n+1}^{\uparrow}(L_n). \tag{20}$$

It gives $2(N-1)$ equations. The upper boundary condition is given by the diffuse incident flux F_0 and the lower one by the albedo α_b of the underlying surface, which must be prescribed:

$$F_1^{\downarrow}(0) = F_0 \tag{21}$$

$$F_N^{\uparrow}(L_N) = \alpha_b \left(F_N^{\downarrow}(L_N) + F^{\mathrm{dir}}(L_N) \right). \tag{22}$$

This provides 2 more equations. These $2N$ equations form a linear system with $2N$ unknowns A_n and B_n. The coefficients A_n and B_n are determined by solving the system, which allows explicit calculation of the diffuse fluxes at any depth. This method has been extensively described (Shettle and Weinman, 1970; Wiscombe, 1977; Liou et al., 1988; Toon et al., 1989). The total fluxes are obtained by summing the diffuse and direct fluxes. The albedo is deduced as the ratio of the total upwelling to the total downelling flux at the surface.

2.4 Impurities

Equations (10) and (11) have been derived assuming pure snow. However, light absorbing impurities, such as black carbon (BC) (e.g. Warren and Wiscombe, 1980; Flanner et al., 2012), dust (Warren and Wiscombe, 1980; Painter et al., 2007) and HULIS (Hoffer et al., 2006; France et al., 2012), impact snow optical properties, especially in the visible range (Warren and Wiscombe, 1980; Reay et al., 2012). These impurities are taken into account in TARTES. Whether impurities are inside or external to ice grains is critical to model their impact. However little is known about it (Flanner et al.,

TCD
7, 2801–2843, 2013

2012). We assume that they are external to ice grains, and that summarizing rules are valid (Warren and Wiscombe, 1980). This hypothesis has been questioned in several papers (e.g. Chýlek et al., 1983; Bohren, 1986). We also assume that these particles are small compared to the wavelength and that they do not affect the total phase function. In contrast, they have a strong influence on the absorption coefficient. The absorption cross section C^i_{abs} of a small spherical impurity of type i is proportionnal to the particle volume V_i and depends on the complex refractive index m_i (Kokhanovsky, 2004):

$$C^i_{\text{abs}} = -\frac{6\pi}{\lambda} V_i \text{Im}\left(\frac{m_i^2 - 1}{m_i^2 + 2}\right). \tag{23}$$

The total absorption coefficient is:

$$\sigma_{\text{abs}} = C^{\text{snow}}_{\text{abs}} n_{\text{snow}} + \sum_i C^i_{\text{abs}} n_i, \tag{24}$$

where n_i is the number density of impurity i particles (m^{-3}) and can be expressed as $n_i = \frac{\rho_i}{\rho_i^0 V_i}$, where ρ_i^0 is the bulk density and ρ_i the impurity concentration ($\text{kg}\,\text{m}^{-3}$). The latter is related to the impurity content by $c_i = \frac{\rho_i}{\rho_{\text{snow}}}$ ($\text{kg}\,\text{kg}^{-1}$). For low impurity contents, we assume that scattering is essentially due to ice grains, and that σ_{e} is unaltered. In that case, Eq. (6) is replaced by:

$$(1 - \omega) = \frac{V}{2\Sigma}\left[B\gamma - \frac{6\pi}{\lambda}\rho_{\text{ice}} \sum_i \frac{c_i}{\rho_i^0} \text{Im}\left(\frac{m_i^2 - 1}{m_i^2 + 2}\right)\right]. \tag{25}$$

To summarize, TARTES takes as inputs for each layer the density, depth, B, $\Sigma(1 - g^{\text{G}})/V$ (or $\text{SSA}(1-g^{\text{G}})$ if the particles are convex), the type and content of impurities. In addition, the direct and diffuse incident fluxes and the albedo of the underlying surface

TCD
7, 2801–2843, 2013

are required. The model computes the internal fluxes at any depth, from which the absorbed energy can be determined for each layer. The e-folding depth $\ell(\lambda)$ between two depths z_1 and z_2 (with $z_2 > z_1$) is calculated at any wavelength as:

$$\ell(\lambda) = \frac{1}{z_2 - z_1} \ln\left(\frac{F^{\downarrow}(z_1,\lambda)}{F^{\downarrow}(z_2,\lambda)}\right). \quad (26)$$

To evaluate TARTES, we compared it to DISORT (Stamnes et al., 1988) simulations run with a monodispersion of spherical particles (Wiscombe, 1980). To this end we chose $B = 1.25$ and $g^{\mathrm{G}} = 0.79$ in our model. For a large set of snowpacks with BC content varying from 1 to 1000 $\mathrm{ng\,g^{-1}}$ and SSA varying from 5 to 100 $\mathrm{m^2\,kg^{-1}}$, we imposed various incident light conditions, mixing diffuse light and direct light with zenith angle ranging from 0° to 85°. The spectral relative error between albedos and fluxes calculated with TARTES and those predicted by DISORT was lower than 3 %.

3 Theoretical calculations of B and g^{G} for various grain shapes

In the theory described in Sect. 2, snow grain shape is fully described by two parameters: B and g^{G}. Values of these parameters for geometric shapes are scarce in the literature. We gather values from the literature and from our calculations (for an extended set of geometric shapes), and we analyze the range of variations.

Monte Carlo ray tracing methods have been used by Takano and Liou (1989); Mishchenko et al. (1996); Macke et al. (1996); Xie et al. (2006) to determine single-scattering properties of ice particles in clouds. These studies showed that the phase function, single-scattering albedo and asymmetry factor largely depend on grain shape. The parameters B and g^{G} were calculated for spheroids, hexagonal plates and fractal particles by Kokhanovsky and Macke (1997) and Kokhanovsky and Zege (2004) using ray tracing. In addition, we have performed calculations for cubes, cuboids, cylinders and depth hoar using the ray tracing model SnowRat (Picard et al., 2009) as follows.

TCD
7, 2801–2843, 2013

Photons are launched from different locations on one grain and their trajectories within the grain are calculated assuming geometric optics laws with optical index of ice at 900 nm. The process is repeated for 10^6 photons and 10^4 different grain orientations. g^G is then computed by averaging the cosine of the deviation angle of photons that have escaped the grain. ω is the ratio of photons that have escaped the grain with respect to the number of launched photons. Σ and V are directly computed in SnowRat and B is deduced using Eq. (6). We studied shapes with aspect ratio between 0.25 and 4, as defined in Picard et al. (2009). The values of B and g^G for these shapes are summarized in Table 1 and reported in Fig. 1.

In Fig. 1a, $(1-g^G)$ is plotted as a function of B for all shapes (the quantity $(1-g^G)$ rather than g^G is used, to reflect the dependence in Eqs. (10) and (11)). For the tested shapes, B varies from 1.25 to 2.09 and is minimum for spheres. g^G varies from 0.50 to 0.80. The relative variations of $(1-g^G)$ are larger than those of B. For spheres, $g^G = 0.79$ and $B = 1.25$, highlighting great forward-scattering and weak absorption enhancement. For most of the hexagonal plates they studied, Grenfell et al. (2005) noticed that the asymmetry parameter was lower than that of spheres. Jin et al. (2008) also point out that the spherical assumption overestimates the forward reflected radiances compared to measurements performed in Antarctica by Hudson et al. (2006). They attribute this to the forward peak of the scattering phase function of spheres.

We examine then the influence of grain shape on snow macroscopic optical properties. Since the albedo depends on the quotient $B/(1-g^G)$ and the AFEC on the product $B(1-g^G)$, Fig. 1b shows an alternative representation of Fig. 1a. In this representation, two snowpacks composed of grains with shapes that have the same abscissa (respectively ordinate) have the same AFEC (respectively albedo). The vertical (respectively horizontal) line shows the shapes that have the same extinction (respectively reflectance) properties as spheres. These lines are "iso-extinction" and "iso-albedo" and are also plotted in Fig. 1a. Figure 1b shows that snow grains with equal SSA but different shape can yield very different AFEC (given Eq. (14), the relative difference is 85 %

TCD
7, 2801–2843, 2013

between fractals and spheres of same SSA). As for the albedo, at $\lambda = 1310\,\mathrm{nm}$ and $\mathrm{SSA} = 20\,\mathrm{m^2\,kg^{-1}}$ for instance, the maximum relative difference is 37 % (see Eq. 15). Therefore the spherical assumption may be adequate for computing the albedo of a snowpack, but for the same snowpack may be inadequate for extinction modeling. For instance, spheroids with aspect ratio 0.5 (labeled in Fig. 1) are very similar to spheres in terms of albedo, but not in terms of AFEC. In Fig. 1b, shapes are distributed above and below the horizontal line, suggesting that spheres yield a median albedo with respect to the the other shapes. This might explain the success of the spherical assumption for albedo calculations (e.g., Grenfell et al., 1994). In that calculations, the quotient $B/(1-g^{\mathrm{G}})$ in natural snow is assumed equal to that of spheres. In contrast, for extinction calculations, the spheres appear to be an extreme case, since the AFEC is miminum for spheres. Although settled snow that has experienced metamorphism is unlikely to look like geometric crystals (Bohren, 1983), this suggests that the spherical assumption is a shortcoming for extinction modeling.

4 Experimental determination of B from optical measurements

In this section we propose two methods to retrieve B from optical measurements. The first method assumes a single homogeneous layer. It is relevant for data from the literature (Sect. 4.3.2) for which a detailed stratigraphy of the snowpack is absent. The second method treats the case of a multi-layer snowpack and uses field measurements we have performed for this special purpose.

4.1 Method

Method 1: Knowledge of the AFEC, k_{e}, and the albedo, α, of a homogeneous snow layer allows calculation of the value of B by using Eq. (12) for pure snow, or Eqs. (8), (9) and (25) if light absorbing-impurities are present.

TCD
7, 2801–2843, 2013

Method 2: A more advanced approach can be developed for a layered snowpack, when vertical profiles of density, $\rho(z)$, reflectance at 1310 nm, $\alpha(z)$, and spectral intensity, $I(z,\lambda)$ are measured. Using the TARTES model, an iterative procedure is completed to find the values of B and BC content that produce the best match between the modeled and measured intensity profiles at two different wavelengths λ_1 and λ_2 (where $\lambda_2 > \lambda_1$), or similarly between the modeled and measured spectral e-folding depths within a particular layer. Values of λ_1 and λ_2 are chosen so that snow optical properties at λ_1 are much more sensitive to impurity content than at λ_2. The greater the difference between ice absorption at λ_1 and λ_2, the faster the convergence of the iterative process. Each numerical layer of TARTES is 1 cm-thick. For each layer, the density, $\Sigma(1-g^{G})/V$, B, the type and content of impurities must be specified. The density and reflectance at 1310 nm are measured, while B and impurity contents are unknown parameters. B is assumed uniform within the snowpack. Regarding impurities, only BC is considered since it is largely responsible for snow absorption at $\lambda \geq 600$ nm (Warren, 1984; Sergent et al., 1993; France et al., 2011a). BC refractive index is taken from Chang and Charalampopoulos (1990) and BC density is assigned to 1000 kg m^{-3} (Warren and Wiscombe, 1980). TARTES also requires the albedo of the underlying surface α_b and the direct and diffuse incident fluxes F_0^{direct} and F_0^{diffuse}. It computes the downwelling and upwelling fluxes $F^{\downarrow}_{\text{model}}(z,\lambda)$ and $F^{\uparrow}_{\text{model}}(z,\lambda)$ within a plane-parallel multi-layer snowpack. α_b is set to 1 here. This assumption has no incidence on the intensity calculations for the top 30 cm (maximum depth of our measurements) since we simulated at least 1-m-deep snowpacks. Intensity measurements are taken at depths greater than 3 cm. At such depths, the flux is entirely diffuse in the visible and NIR range (Barkstrom, 1972), so we can take $F_0^{\text{direct}} = 0$, $F_0^{\text{diffuse}} = F_0(\lambda)$ without loss of generality. $F_0(\lambda)$ is an unknown parameter. The iterative method to retrieve the optimal B_{opt}, BC_{opt} and $F_0(\lambda)$ follows a three-step procedure:

1. The measured intensity profile at λ_2 is used to find a first guess for B, assuming $\text{BC}_0 = 100\,\text{ng g}^{-1}$. For each pair ($B$, $F_0(\lambda_2)$) in the range of optimization,

TCD
7, 2801–2843, 2013

$\Sigma(1 - g^G)/V$ is deduced for each layer from the reflectance profile using Eq. (11) and an intensity profile is computed (B is varied in the range 0.5–2.5 with an increment of 0.1 and $F_0(\lambda_2)$ is varied a factor 10 around the intensity obtained from exponential extrapolation of the measurements at the surface). To measure the quality of the simulation, we consider two error metrics depending on the available measurements.

Case 1: The intensity profile is measured. The difference ϵ_1 between the measured and modeled profiles is calculated as:

$$\epsilon_1(\lambda_2) = \sqrt{\frac{1}{m}\sum_{n=1}^{m}\left(\ln(F^{\downarrow}_{\text{model}}(z_n,\lambda_2)) - \ln(I(z_n,\lambda_2))\right)^2} \tag{27}$$

where z_n is the depth where measurement n was taken and $I(z_n,\lambda)$ the modeled intensity at that depth.

Case 2: If only the spectral e-folding depth between two levels is available, the difference is:

$$\epsilon_2(\lambda_2) = |\ell_{\text{model}}(\lambda_2) - \ell_{\text{measure}}(\lambda_2)| \tag{28}$$

The pair $(B, F_0(\lambda_2))$ that minimizes $\epsilon_1(\lambda_2)$ (or $\epsilon_2(\lambda_2)$) provides a first estimate of B in the snowpack.

2. The value of B found at step 1 is used to model the intensity profile at λ_1. The BC content is chosen by minimizing $\epsilon_1(\lambda_1)$ (or $\epsilon_2(\lambda_1)$).

3. The latter value of BC is then used at step 1 to refine B and so on. Iteration using λ_2 and λ_1 is performed until the optimal pair (B, BC) between two iterations does not change. In practice, less than 10 iterations are needed for convergence.

TCD
7, 2801–2843, 2013

The retrieved value of B is sensitive to the precision of the density, reflectance and intensity measurements. In fact the derivation of Eq. (12) reads:

$$\frac{\delta B}{B} \sim \left| \frac{\delta k_e(\lambda_{k_e})}{k_e(\lambda_{k_e})} \right| + \left| \frac{\delta \ln(\alpha(\lambda_\alpha))}{\ln(\alpha(\lambda_\alpha))} \right| + \left| \frac{\delta \rho}{\rho} \right|. \quad (29)$$

It highlights the high sensitivity of B retrieval to the reflectance measurement if reflectance is close to 1. The larger λ_α, the lower $\alpha(\lambda_\alpha)$ and the greater the precision of B retrieval. Using λ_α = 1310 nm for our measurements is thus more precise than using reflectance measurements in the visible range.

4.2 Materials

A first set of measurements were conducted at Dome C (DC, 75.10° S, 123.33° E, 3233 m a.s.l.), Antarctica, in January 2010. Spectral *e*-folding depths were measured at the same location following the procedure detailed in France et al. (2011a). Density at 3 cm resolution was measured with a rectangular cutting device of volume 300 cm^3 and a 0.3 g precision scale. Profiles of nadir-hemispherical reflectance at 1310 nm were obtained with POSSSUM (Arnaud et al., 2011). The conversion from nadir-hemispherical reflectance $\alpha_{nh}(z)$ to diffuse reflectance $\alpha(z)$ is, following Eq. (1) of Picard et al. (2009):

$$\ln(\alpha(z)) = \frac{7}{9} \ln(\alpha_{nh}(z)). \quad (30)$$

The measurements were conducted in two different layers identified visually. Method 2 (case 2) described in Sect. 4.1 is applied with λ_1 = 500 nm and λ_2 = 700 nm.

The second set of measurements was collected during the winter 2012 at three different sites in the French Alps: Col de Porte (CP, 45.17° N, 5.46° E, 1326 m a.s.l.), Lacs Robert (LR, 45.08° N, 5.55° E, 2000 m a.s.l.), and Lac Poursollet (LP, 45.05° N, 5.90° E, 1658 m a.s.l.). For each site, a 1 m-deep pit was dug in a flat, horizontal and unaltered

TCD
7, 2801–2843, 2013

snow area. $I(z,\lambda)$ is measured with fiber optics as follows. First, 60 cm long horizontal holes with the same diameter as the fibers are prepared at approximately 5 cm intervals from the surface to a maximum depth of 30 cm (a guiding support is used to ensure their horizontality). At greater depth, light entering the snowpack from the pit face pertubs the internal radiation field (Bohren and Barkstrom, 1974; France et al., 2011b). The holes are made in the sun direction in order to avoid shading by the operator. Then, one bare fiber optic with a 25° field-of-view is successively inserted into the holes from the top to the bottom of the snowpack. The fiber is placed 2 cm away from the hole extremity to limit the peturbation due to the presence of the fiber. The spectrum is recorded at each depth with an Ocean Optics MAYA 2000® spectrophotometer with spectral resolution 0.5 nm. Intensity measurement in the uppermost hole is duplicated at the beginning and at the end of the measurement series. Series with variations of the incident flux larger than 3 % were discarded. Profile of density with 5 cm vertical resolution is measured using a cylindrical cutting device of volume 100 cm^3 and a 0.1 g precision scale. Profile of reflectance at 1310 nm is measured at 1-cm resolution with ASSSAP (the Alpine version of POSSSUM), except for the 9 March and Lacs Robert measurements where diffuse reflectance was measured with DUFISSS (Gallet et al., 2009) on samples extracted from the pit face. Method 2 (case 1) is used with λ_1 = 600 nm and λ_2 = 780 nm.

4.3 Results

4.3.1 Application to dedicated measurements

The method 2 presented in Sect. 4.1 is applied to the data collected at Dome C and in the Alps. Table 2 summarizes the values of B and BC retrieved for each set of measurements, along with details on snow type and instruments used. At Dome C, the method yields B = 1.9 for the hard windpack layer and B = 2.0 for the depth-hoar layer. Figure 2a shows the intensity profile at 600 nm measured at Col de Porte on 29 February 2012. Modeled intensity profiles using density and reflectance profiles (Fig. 2b are

TCD
7, 2801–2843, 2013

also plotted for various values of B and constant incident flux. Figure 2a illustrates the sensitivity of light extinction to B. At 20 cm depth, intensity at 600 nm varies by more than 50 % for B ranging from 1.25 to 2.0. With $B = 1.25$ (spheres), intensity at depth is overestimated. The vertical variations of the intensity profile are well reproduced by the model, in particular the changes of slope at 10 and 20 cm. For this experiment, the best match is obtained for $B = 1.9$. Figure 3 shows the measured and modeled intensity profiles at 780 nm for the other Alpine measurements. The optimal modeled profile is symbolized by dark inverted triangles. $B = 1.8$ produces the best match for the 24 February 2012 measurements while $B = 1.6$ was the best for the measurements at Lacs Robert and Lac Poursollet. $B = 0.8$ is found for the fresh snow layer of the the 9 March 2012 measurement. The arrows in Fig. 1a show the 7 values of B, ranging from 0.8 to 2.0, retrieved experimentally. The large range probably explains why the spherical assumption is inadequate for modeling penetration of light in natural snow.

The retrieved BC contents vary from 12 to 85 $\mathrm{ng\,g^{-1}}$ for the Alpine sites, which is in agreement with values between 34 and 247 $\mathrm{ng\,g^{-1}}$ reported by Sergent et al. (1998). BC contents retrieved for Dome C ($\simeq 5\,\mathrm{ng\,g^{-1}}$) are consistent with the 3 $\mathrm{ng\,g^{-1}}$ reported by Warren et al. (2006) for the upper 30 cm of the snowpack and with the values reported by France et al. (2011a). In fact, our method yields an upper limit of BC content since all impurities absorption is attributed to BC, which is certainly not realistic (Zatko et al., 2012). Anyway, we do not aim here at retrieving a real BC content and this assumption does not affect the B estimation since such contents have a negligible impact on snow optical properties at 700 nm (see Fig. 4).

Even though the retrieval method is based only on two wavelengths λ_1 and λ_2, we checked that modeled intensity profiles at other wavelengths were in good agreement with the measured ones. In Fig. 5, the measured and modeled e-folding depths are plotted for Dome C depth-hoar layer and for the upper layer of the snowpack studied at Lacs Robert. Modeled e-folding depths for various values of B are also shown. The relative error is less than 5 % for the whole visible spectrum. In Fig. 5a, the discrepancies

TCD
7, 2801–2843, 2013

between the model and the measurement from 400 nm to 500 nm are probably due to the presence of other types of impurities (France et al., 2011a).

4.3.2 Application to data in the literature

Method 1 was applied to retrieve B using published data. There have been few simultaneous measurements of extinction and reflectance of snow reported in the literature. Earlier studies dealt with broadband extinction (O'Neill and Gray, 1972; Fukami et al., 1985) so that general features were retrieved (such as the increase of the broadband e-folding depth with depth) but no quantitative information on grain shape can be inferred. Studies with spectrally-resolved measurements include the works of Grenfell and Maykut (1977) in Arctic, Beaglehole et al. (1998) in Antarctica, Perovich (2007) on mid-latitude seasonal snow, France et al. (2011a) in Antarctica, France et al. (2011b) in Svalbard and France et al. (2012) in Alaska. Spectral diffuse reflectance and AFEC were measured or deduced from measurements. B values are calculated using Eq. (12) for all these cases.

A wide range of B is obtained, from 1.0 to 9.9. Experimental details and B values for each study are summarized in Table 3. The wavelengths used in Eq. (12) are specified since they depend on available data. B values are also reported in Fig. 6, along with the values based on our measurements and those resulting from theoretical calculations. Some of the values obtained from the literature exceed the range obtained from theoretical calculations and dedicated measurements. Intuitively, high B values, i.e. high lengthening of the photon path within the grain, are only possible with specific shapes that trap the light, like fiber optics. Uncertainty in the measurements is a potential cause of these high values. In fact, Eq. (12) is applied with $700\,\text{nm} < \lambda_\alpha < 900\,\text{nm}$, so that $\alpha(\lambda_\alpha)$ is generally close to 1 and the uncertainty of the retrieved value of B is large (see Eq. 29). In Table 3, the 5 largest B values are underlined. They are obtained for the lowest values of α. This may indicate that Eq. (12) cannot be applied to wet or old coarse snow with low albedo, or that impurities amounts in these studies were too large for Eq. (12) to be be applied. This may also indicate that accurate

TCD
7, 2801–2843, 2013

reflectance measurements are more difficult than *e*-folding depth measurements. The spectral resolution of the instruments and the quality of the diffuse incident flux may also been accounted for.

5 Discussion

According to Koh (1989), "until the phase function of snow is known, the use of a spherical equivalent phase function may be the most appropriate". Although the spherical assumption has proved successful for albedo modeling, it is much less appropriate for light extinction modeling. The following discussion will explore the failure of the spherical grain assumption for extinction data.

To model light extinction in snow, we developed a radiative transfer model, called TARTES, based on the AART theory. In this model snow grains are characterized by their SSA, and two shape parameters B and g^{G}. The absorption enhancement parameter B quantifies the lengthening of photon paths inside a snow grain due to internal multiple reflections, and the asymmetry factor g^{G} quantifies the forward-scattering of light by the snow grain. Theoretical calculations performed in Sect. 3 show that spheres are highly forward-scattering (large g^{G}) and weakly absorbing (small B). Spheres are very singular among different other geometric grain shapes, explaining the difficulty to match light extinction measurements with models using spherical grains (e.g. Sergent et al., 1987; Meirold-Mautner and Lehning, 2004). Qualitatively, when B is large in a medium, photons are internally reflected several times in a grain before escaping, and are then likely to exit the grain in no particular direction. Conversely, when B is small, photons travel a minimal distance in the grain, i.e. they tend to exit at the opposite point of their entry, and tend to be scattered preferentially in the forward direction, which leads to large g^{G}. Thus B and $(1-g^{\mathrm{G}})$ are correlated. An important consequence is that the quotient $B/(1-g^{\mathrm{G}})$ – that determines the albedo – should be relatively constant with respect to grain morphology while the product $B(1-g^{\mathrm{G}})$ – that is important

TCD
7, 2801–2843, 2013

for the extinction – varies widely. The numerical calculations presented in Fig. 1 confirm this analysis. This can be further explained by the fact that in snow with a large value of B, photons tend (i) to travel a long way within the ice grains (which increases likelihood of absorption) and (ii) to be scattered in all directions, including the backward direction. The penetration depth of the photons is limited because absorption is enhanced and because forward-scattering is reduced. Regarding the albedo, as the probability that a photon escapes the snowpack before being absorbed, photons in snow with large B are scattered in all directions and are likely to escape the medium after fewer scattering events than in snow with small B. However, this is counterbalanced by the higher probability of absorption between scattering events in snow with large B, because the path in the grains is longer. In short, the increase of photons paths within the grains for larger B is counterbalanced by the shortening of total path lengths in the snowpack due to lower g^{G}. This explains the limited sensitivity of albedo to the shape of the grains. The low sensitivity was noticed experimentally by Domine et al. (2006) who studied snow samples with various crystal shapes and confirmed later by Gallet et al. (2009). They demonstrate indeed that the reflectance of snow samples of known SSA (Dominé et al., 2001) is well reproduced using DISORT-Mie code (Wiscombe, 1980; Stamnes et al., 1988), i.e. for a medium of independent spheres.

In this paper, we exploit the sensitivity of light extinction to estimate the grain shape parameter B using measurements of reflectance, density and profiles of intensity within the snowpack, and TARTES model. The values of B – obtained by minimizing the difference between measured and modeled profiles – are generally greater than the value for spheres ($B = 1.25$). It means that assuming spherical grains in snow models leads to an overestimation of the e-folding depth. Spheres are thus inappropriate to model light extinction in natural snow. By sampling different snow types, we found that old snow with large grains has a B close to that of spheroids with aspect ratio 0.7 (see Table 1). Snow in Antarctica, that is facetted, has values around 1.9, which is also the case of hexagonal plates. Fine grains have intermediate values ($1.6 \leq B \leq 1.9$), probably because they are composed of a mixture of rounded and regular faces. The result

TCD
7, 2801–2843, 2013

for fresh snow is more surprising. Indeed, the value $B = 0.8$ is incompatible with the definition of B (Kokhanovsky, 2004) that constrains its value to be larger than 1. Inaccurate measurements, or the small size of fresh snow crystals, close to the wavelength, for which geometric optics does not apply, may be the cause of this invalid estimation. Shadowing effects and interparticle interference (Wiscombe and Warren, 1980; Warren, 1982; Kokhanovsky, 2004), that are not taken into account in the model, may also explain this value of B. Except for fresh snow, the values of B obtained from our measurements are coherent with the values predicted by theoretical calculations (Fig. 6). In contrast, the values deduced from the literature vary in a large extent. In fact, the sensitivity of the retrieval method to the measurements, illustrated by Eq. (29), points out that measurements should be taken carefully, and at appropriate wavelengths. We recommend not to consider these latter B values in the future.

Although there is no mention of experimental determination of B in the literature to compare with our results, some studies explicitly mention the asymmetry factor g. Figure 4 of Bohren and Barkstrom (1974) compares AFEC measurements of Liljequist (1956) to a two-stream model and shows that the e-folding depth modeled with spheres is greater than that measured, and that $g^{\mathrm{G}} = 0.68$ should be used for better agreement. Meirold-Mautner and Lehning (2004) show that taking $g^{\mathrm{G}} = 0.72$ instead of 0.78 in their model allows a better fit with measurements. Kokhanovsky and Zege (2004) suggest $g^{\mathrm{G}} = 0.5$, based on measurements on ice particles in clouds (Garrett et al., 2001; Barkey et al., 2002), and calculations on fractal particles described in Macke et al. (1996). Under the assumption that $B/(1 - g^{\mathrm{G}})$ is nearly independent of grain shape for natural snow, and equal to that for spheres, a rough estimate of g^{G} can be obtained from B values. Based on our B measurements (excluding fresh snow which gives erroneous B), the range of g^{G} would be 0.66–0.73. These values are in agreement with previous studies. However, in most of these studies, geometric grain size was estimated from visual observation of grains which can differ from the optical grain size that determines snow optical properties (Langlois et al., 2010). Our approach is more accurate in that it does not use snow grain size but reflectance at 1310 nm.

TCD
7, 2801–2843, 2013

Reflectance can be measured more accurately and less subjectively than grain size, especially for non spherical particles.

6 Conclusions

The present paper shows that for light extinction modeling, spheres are inappropriate to represent natural snow. Indeed, theoretical calculations as well as measurements point out that the absorption enhancement parameter B is greater for natural snow than for spheres. As a consequence, the asymmetry factor g^{G} in natural snow is probably lower than that of spheres, and modeled e-folding depth is overestimated when grains are assumed spherical, which is in agreement with observations from the literature. Grain shape is highly variable with time and location (Colbeck, 1982), hence snow cannot be systematically represented by a collection of spheres. To account for the grain shape in optical radiative transfer models, such as those used in weather forecast and climate models, we need to further explore the relationship between B and snow type or traditional snow grain shape (Fierz et al., 2009). To this end future work should focus on the systematic determination of B in laboratory and in the field. In addition, a method to determine g^{G} should be developed which will require independent measurements of SSA.

Acknowledgements. This study was supported by the ANR MONISNOW programme. We are grateful to the French Polar Institute (IPEV) for the logistic support at Concordia station in Antarctica through the CALVA and NiteDC programmes. J. L. F. and M. D. K. thank NERC for support through grants NE/F0004796/1, NE/F010788 and NERC FSF for support through grants 555.0608, 584.0609 and support from Royal Holloway Earth Sciences research strategy fund awards.

TCD
7, 2801–2843, 2013

The publication of this article
is financed by CNRS-INSU.

References

Aoki, T., Aoki, T., Fukabori, M., Hachikubo, A., Tachibana, Y., and Nishio, F.: Effects of snow physical parameters on spectral albedo and bidirectional reflectance of snow surface, J. Geophys. Res., 105, 10219–10236, doi:10.1029/1999JD901122, 2000. 2804

Arnaud, L., Picard, G., Champollion, N., Domine, F., Gallet, J., Lefebvre, E., Fily, M., and Barnola, J.: Measurement of vertical profiles of snow specific surface area with a 1 cm resolution using infrared reflectance: instrument description and validation, J. Glaciol., 57, 17–29, doi:10.3189/002214311795306664, 2011. 2818

Barkey, B., Bailey, M., Liou, K.-N., and Hallett, J.: Light-scattering properties of plate and column ice crystals generated in a laboratory cold chamber, Appl. Optics, 41, 5792–5796, doi:10.1364/AO.41.005792, 2002. 2824

Barkstrom, B. R.: Some effects of multiple scattering on the distribution of solar radiation in snow and ice, J. Glaciol., 11, 357–368, available at: http://adsabs.harvard.edu/abs/1972JGlac..11..357B, 1972. 2816

Beaglehole, D., Ramanathan, B., and Rumberg, J.: The UV to IR transmittance of Antarctic snow, J. Geophys. Res., 103, 8849–8857, doi:10.1029/97JD03604, 1998. 2821, 2837

Bohren, C. F.: Colors of snow, frozen waterfalls, and icebergs, J. Opt. Soc. Am., 73, 1646–1652, doi:10.1364/JOSA.73.001646, 1983. 2815

Bohren, C. F.: Applicability of effective-medium theories to problems of scattering and absorption by nonhomogeneous atmospheric particles, J. Atmos. Sci., 43, 468–475, doi:10.1175/1520-0469(1986)043<0468:AOEMTT>2.0.CO;2, 1986. 2812

Bohren, C. F. and Barkstrom, B. R.: Theory of the optical properties of snow, J. Geophys. Res., 79, 4527–4535, doi:10.1029/JC079i030p04527, 1974. 2804, 2806, 2808, 2810, 2819, 2824

TCD
7, 2801–2843, 2013

Brandt, R. E. and Warren, S. G.: Solar-heating rates and temperature profiles in Antarctic snow and ice, J. Glaciol., 39, 99–110, available at: http://adsabs.harvard.edu/abs/1993JGlac..39...99B, 1993. 2803, 2804, 2808

Brun, E., Martin, E., Simon, V., Gendre, C., and Coléou, C.: An energy and mass model of snow cover suitable for operational avalanche forecasting, J. Glaciol., 35, 333–342, available at: http://adsabs.harvard.edu/abs/1989JGlac..35..333B, 1989. 2804

Brun, E., David, P., Sudul, M., and Brunot, G.: A numerical model to simulate snow-cover stratigraphy for operational avalanche forecasting, J. Glaciol., 38, 13–22, available at: http://adsabs.harvard.edu/abs/1992JGlac..38...13B, 1992. 2804

Cess, R. D., Potter, G. L., Zhang, M.-H., Blanchet, J.-P., Chalita, S., Colman, R., Dazlich, D. A., del Genio, A. D., Dymnikov, V., Galin, V., Jerrett, D., Keup, E., Lacis, A. A., Le Treut, H., Liang, X.-Z., Mahfouf, J.-F., McAvaney, B. J., Meleshko, V. P., Mitchell, J. F. B., Morcrette, J.-J., Norris, P. M., Randall, D. A., Rikus, L., Roeckner, E., Royer, J.-F., Schlese, U., Sheinin, D. A., Slingo, J. M., Sokolov, A. P., Taylor, K. E., Washington, W. M., Wetherald, R. T., and Yagai, I.: Interpretation of snow–climate feedback as produced by 17 general circulation models, Science, 253, 888–892, doi:10.1126/science.253.5022.888, 1991. 2803

Chandrasekhar, S.: Radiative Transfer, Courier Dover Publications, 1960. 2803, 2806

Chang, H. and Charalampopoulos, T. T.: Determination of the wavelength dependence of refractive indices of flame soot, Royal Society of London Proceedings Series A, 430, 577–591, available at: http://adsabs.harvard.edu/abs/1990RSPSA.430..577C, 1990. 2816

Chýlek, P., Ramaswamy, V., and Srivastava, V.: Albedo of soot-contaminated snow, J. Geophys. Res., 88, 10837–10843, doi:10.1029/JC088iC15p10837, 1983. 2812

Colbeck, S.: Snow-crystal growth with varying surface temperatures and radiation penetration, J. Glaciol., 35, 23–29, doi:10.3189/002214389793701536, 1989. 2803

Colbeck, S. C.: An overview of seasonal snow metamorphism (Paper 1R1414), Rev. Geophys., 20, 45–61, doi:10.1029/RG020i001p00045, 1982. 2803, 2825

Dominé, F., Cabanes, A., Taillandier, A.-S., and Legagneux, L.: Specific surface area of snow samples determined by CH_4 adsorption at 77 K and estimated by optical microscopy and scanning electron microscopy, Environ. Sci. Technol., 35, 771–780, doi:10.1021/es001168n, 2001. 2810, 2823

Domine, F., Salvatori, R., Legagneux, L., Salzano, R., Fily, M., and Casacchia, R.: Correlation between the specific surface area and the short wave infrared (SWIR) reflectance of snow, Cold Reg. Sci. Technol., 46, 60–68, doi:10.1016/j.coldregions.2006.06.002, 2006. 2823

TCD
7, 2801–2843, 2013

Domine, F., Albert, M., Huthwelker, T., Jacobi, H.-W., Kokhanovsky, A. A., Lehning, M., Picard, G., and Simpson, W. R.: Snow physics as relevant to snow photochemistry, Atmos. Chem. Phys., 8, 171–208, doi:10.5194/acp-8-171-2008, 2008. 2803

Dumont, M., Brissaud, O., Picard, G., Schmitt, B., Gallet, J.-C., and Arnaud, Y.: High-accuracy measurements of snow Bidirectional Reflectance Distribution Function at visible and NIR wavelengths – comparison with modelling results, Atmos. Chem. Phys., 10, 2507–2520, doi:10.5194/acp-10-2507-2010, 2010. 2804

Dunkle, R. V. and Bevans, J. T.: An approximate analysis of the solar reflectance and transmittance of a snow cover, J. Meteorol., 13, 212–216, doi:10.1175/1520-0469(1956)013<0212:AAAOTS>2.0.CO;2, 1956. 2805, 2810

Fierz, C., Armstrong, R. L., Durand, Y., Etchevers, P., Greene, E., McClung, D. M., Nishimura, K., Satyawali, P. K., and Sokratov, S. A.: The International Classification for Seasonal Snow on the Ground, UNESCO/IHP, 2009. 2825

Flanner, M. G.: Snowpack radiative heating: influence on Tibetan Plateau climate, Geophys. Res. Lett., 32, L06501, doi:10.1029/2004GL022076, 2005. 2803

Flanner, M. G., Liu, X., Zhou, C., Penner, J. E., and Jiao, C.: Enhanced solar energy absorption by internally-mixed black carbon in snow grains, Atmos. Chem. Phys., 12, 4699–4721, doi:10.5194/acp-12-4699-2012, 2012. 2811

Flin, F., Brzoska, J.-B., Lesaffre, B., Coléou, C., and Pieritz, R. A.: Three-dimensional geometric measurements of snow microstructural evolution under isothermal conditions, Ann. Glaciol., 38, 39–44, doi:10.3189/172756404781814942, 2004. 2810

France, J. and King, M.: The effect of measurement geometry on recording solar radiation attenuation in snowpack (e-folding depth) using fibre-optic probes, J. Glaciol., 58, 417–418, doi:10.3189/2012JoG11J227, 2012. 2805

France, J. L., King, M. D., Frey, M. M., Erbland, J., Picard, G., Preunkert, S., MacArthur, A., and Savarino, J.: Snow optical properties at Dome C (Concordia), Antarctica; implications for snow emissions and snow chemistry of reactive nitrogen, Atmos. Chem. Phys., 11, 9787–9801, doi:10.5194/acp-11-9787-2011, 2011a. 2816, 2818, 2820, 2821, 2837

France, J. L., King, M. D., Lee-Taylor, J., Beine, H. J., Ianniello, A., Domine, F., and MacArthur, A.: Calculations of in-snow NO_2 and OH radical photochemical production and photolysis rates: a field and radiative-transfer study of the optical properties of Arctic (Ny-Ålesund, Svalbard) snow, J. Geophys. Res., 116, F04013, doi:10.1029/2011JF002019, 2011b. 2805, 2819, 2821, 2837

TCD
7, 2801–2843, 2013

France, J. L., Reay, H. J., King, M. D., Voisin, D., Jacobi, H. W., Domine, F., Beine, H., Anastasio, C., MacArthur, A., and Lee-Taylor, J.: Hydroxyl radical and NO_x production rates, black carbon concentrations and light-absorbing impurities in snow from field measurements of light penetration and nadir reflectivity of onshore and offshore coastal Alaskan snow, J. Geophys. Res., 117, D00R12, doi:10.1029/2011JD016639, 2012. 2811, 2821, 2837

Fukami, H., Kojima, K., and Aburakawa, H.: The extinction and absorption of solar radiation within a snow cover, Ann. Glaciol., 6, 118–122, available at: http://adsabs.harvard.edu/abs/1985AnGla...6..118F, 1985. 2821

Gallet, J.-C., Domine, F., Zender, C. S., and Picard, G.: Measurement of the specific surface area of snow using infrared reflectance in an integrating sphere at 1310 and 1550 nm, The Cryosphere, 3, 167–182, doi:10.5194/tc-3-167-2009, 2009. 2804, 2819, 2823

Garrett, T. J., Hobbs, P. V., and Gerber, H.: Shortwave, single-scattering properties of arctic ice clouds, J. Geophys. Res., 106, 15155–15172, doi:10.1029/2000JD900195, 2001. 2824

Giddings, J. C. and LaChapelle, E.: Diffusion theory applied to radiant energy distribution and albedo of snow, J. Geophys. Res., 66, 181–189, doi:10.1029/JZ066i001p00181, 1961. 2805

Grenfell, T. C. and Maykut, G. A.: The optical properties of ice and snow in the Arctic Basin, J. Glaciol., 18, 445–463, available at: http://adsabs.harvard.edu/abs/1977JGlac..18..445G, 1977. 2821, 2837

Grenfell, T. C. and Warren, S. G.: Representation of a nonspherical ice particle by a collection of independent spheres for scattering and absorption of radiation, J. Geophys. Res., 104, 31697–1709, doi:10.1029/1999JD900496, 1999. 2804

Grenfell, T. C., Warren, S. G., and Mullen, P. C.: Reflection of solar radiation by the Antarctic snow surface at ultraviolet, visible, and near-infrared wavelengths, J. Geophys. Res., 99, 18669–18684, doi:10.1029/94JD01484, 1994. 2815

Grenfell, T. C., Neshyba, S. P., and Warren, S. G.: Representation of a nonspherical ice particle by a collection of independent spheres for scattering and absorption of radiation: 3. Hollow columns and plates, J. Geophys. Res., 110, D17203, doi:10.1029/2005JD005811, 2005. 2804, 2814

Hall, A.: The role of surface albedo feedback in climate, J. Climate, 17, 1550–1568, doi:10.1175/1520-0442(2004)017<1550:TROSAF>2.0.CO;2, 2004. 2803

Hall, A. and Qu, X.: Using the current seasonal cycle to constrain snow albedo feedback in future climate change, Geophys. Res. Lett., 33, L03502, doi:10.1029/2005GL025127, 2006. 2803

TCD
7, 2801–2843, 2013

Hoffer, A., Gelencsér, A., Guyon, P., Kiss, G., Schmid, O., Frank, G. P., Artaxo, P., and Andreae, M. O.: Optical properties of humic-like substances (HULIS) in biomass-burning aerosols, Atmos. Chem. Phys., 6, 3563–3570, doi:10.5194/acp-6-3563-2006, 2006. 2811

Hudson, S. R., Warren, S. G., Brandt, R. E., Grenfell, T. C., and Six, D.: Spectral bidirectional reflectance of Antarctic snow: measurements and parameterization, J. Geophys. Res., 111, D18106, doi:10.1029/2006JD007290, 2006. 2814

Jiménez-Aquino, J. I. and Varela, J. R.: Two stream approximation to radiative transfer equation: an alternative method of solution, Rev. Mex. Fis., 51, 82–86, available at: http://adsabs.harvard.edu/abs/2005RMxF...51...82J, 2005. 2810

Jin, Z., Charlock, T. P., Yang, P., Xie, Y., and Miller, W.: Snow optical properties for different particle shapes with application to snow grain size retrieval and MODIS/CERES radiance comparison over Antarctica, Remote Sens. Environ., 112, 3563–3581, doi:10.1016/j.rse.2008.04.011, 2008. 2814

Joseph, J. H., Wiscombe, W. J., and Weinman, J. A.: The delta-Eddington approximation for radiative flux transfer, J. Atmos. Sci., 33, 2452–2459, doi:10.1175/1520-0469(1976)033<2452:TDEAFR>2.0.CO;2, 1976. 2806, 2810

King, M. D. and Simpson, W. R.: Extinction of UV radiation in Arctic snow at Alert, Canada (82° N), J. Geophys. Res., 106, 12499–12507, doi:10.1029/2001JD900006, 2001. 2803, 2810

Koh, G.: Radiative Transfer in Falling Snow: a Two-Stream Approximation, Tech. rep., available at: http://adsabs.harvard.edu/abs/1989rtfs.rept.....K, 1989. 2822

Kokhanovsky, A. A.: Light Scattering Media Optics: Problems and Solutions, Springer, 2004. 2806, 2808, 2812, 2824

Kokhanovsky, A. A. and Macke, A.: Integral light-scattering and absorption characteristics of large, nonspherical particles, Appl. Optics, 36, 8785–8790, doi:10.1364/AO.36.008785, 1997. 2805, 2813, 2835

Kokhanovsky, A. A. and Zege, E. P.: Scattering optics of snow, Appl. Optics, 43, 1589–1602, doi:10.1364/AO.43.001589, 2004. 2804, 2805, 2806, 2807, 2808, 2813, 2824

Kuipers Munneke, P., van den Broeke, M. R., Reijmer, C. H., Helsen, M. M., Boot, W., Schneebeli, M., and Steffen, K.: The role of radiation penetration in the energy budget of the snowpack at Summit, Greenland, The Cryosphere, 3, 155–165, doi:10.5194/tc-3-155-2009, 2009. 2803

TCD
7, 2801–2843, 2013

Kuipers Munneke, P., van den Broeke, M. R., King, J. C., Gray, T., and Reijmer, C. H.: Near-surface climate and surface energy budget of Larsen C ice shelf, Antarctic Peninsula, The Cryosphere, 6, 353–363, doi:10.5194/tc-6-353-2012, 2012. 2804

Langlois, A., Royer, A., Montpetit, B., Picard, G., Brucker, L., Arnaud, L., Harvey-Collard, P., Fily, M., and Goïta, K.: On the relationship between snow grain morphology and in-situ near infrared calibrated reflectance photographs, Cold Reg. Sci. Technol., 61, 34–42, doi:10.1016/j.coldregions.2010.01.004, 2010. 2824

Lee-Taylor, J. and Madronich, S.: Calculation of actinic fluxes with a coupled atmosphere-snow radiative transfer model, J. Geophys. Res., 107, 4796, doi:10.1029/2002JD002084, 2002. 2803

Liljequist, G. H.: Energy Exchange of an Antarctic Snow-Field, Vol. 1, Norsk Polarinstitutt, Oslo, available at: http://www.sudoc.fr/102691800, 1956. 2824

Liou, K.-N., Fu, Q., and Ackerman, T. P.: A simple formulation of the delta-four-stream approximation for radiative transfer parameterizations, J. Atmos. Sci., 45, 1940–1948, doi:10.1175/1520-0469(1988)045<1940:ASFOTD>2.0.CO;2, 1988. 2811

Liston, G. E. and Winther, J.-G.: Antarctic surface and subsurface snow and ice melt fluxes, J. Climate, 18, 1469–1481, doi:10.1175/JCLI3344.1, 2005. 2803

Macke, A., Mueller, J., and Raschke, E.: Single scattering properties of atmospheric ice crystals, J. Atmos. Sci., 53, 2813–2825, doi:10.1175/1520-0469(1996)053<2813:SSPOAI>2.0.CO;2, 1996. 2805, 2813, 2824

Meirold-Mautner, I. and Lehning, M.: Measurements and model calculations of the solar shortwave fluxes in snow on Summit, Greenland, Ann. Glaciol., 38, 279–284, doi:10.3189/172756404781814753, 2004. 2805, 2822, 2824

Melnikova, I.: Range of application of the scattering theory within the multicomponent turbid media of the cloud atmosphere is the reason for anomalous absorption and incorrectness of climate prediction, Int. J. Remote Sens., 29, 2615–2628, doi:10.1080/01431160701767443, 2008. 2807

Mie, G.: Beiträge zur Optik trüber Medien, speziell kolloidaler Metallösungen, Ann. Phys.-Berlin, 330, 377–445, doi:10.1002/andp.19083300302, 1908. 2804

Mishchenko, M. I., Travis, L. D., and Macke, A.: Scattering of light by polydisperse, randomly oriented, finite circular cylinders, Appl. Optics, 35, 4927–4940, doi:10.1364/AO.35.004927, 1996. 2813

TCD
7, 2801–2843, 2013

Negi, H. S. and Kokhanovsky, A.: Retrieval of snow albedo and grain size using reflectance measurements in Himalayan basin, The Cryosphere, 5, 203–217, doi:10.5194/tc-5-203-2011, 2011. 2804

Neshyba, S. P., Grenfell, T. C., and Warren, S. G.: Representation of a nonspherical ice particle by a collection of independent spheres for scattering and absorption of radiation: 2. Hexagonal columns and plates, J. Geophys. Res., 108, 4448, doi:10.1029/2002JD003302, 2003. 2804

O'Neill, A. D. J. and Gray, D. M.: Solar radiation penetration through snow, in: International Symposia on the Role of Snow and Ice in Hydrology, vol. 1, available at: http://iahs.info/redbooks/a107/107019.pdf, 227–241 , 1972. 2821

Painter, T. H., Barrett, A. P., Landry, C. C., Neff, J. C., Cassidy, M. P., Lawrence, C. R., McBride, K. E., and Farmer, G. L.: Impact of disturbed desert soils on duration of mountain snow cover, Geophys. Res. Lett., 34, L12502, doi:10.1029/2007GL030284, 2007. 2811

Perovich, D. K.: Light reflection and transmission by a temperate snow cover, J. Glaciol., 53, 201–210, doi:10.3189/172756507782202919, 2007. 2804, 2821, 2837

Picard, G., Arnaud, L., Domine, F., and Fily, M.: Determining snow specific surface area from near-infrared reflectance measurements: numerical study of the influence of grain shape, Cold Reg. Sci. Technol., 56, 10–17, doi:10.1016/j.coldregions.2008.10.001, 2009. 2804, 2805, 2813, 2814, 2818, 2835

Picard, G., Domine, F., Krinner, G., Arnaud, L., and Lefebvre, E.: Inhibition of the positive snow-albedo feedback by precipitation in interior Antarctica, Nat. Clim. Change, 2, 795–798, doi:10.1038/nclimate1590, 2012. 2803

Reay, H. J., France, J. L., and King, M. D.: Decreased albedo, e-folding depth and photolytic OH radical and NO_2 production with increasing black carbon content in Arctic snow, J. Geophys. Res., 117, D00R20, doi:10.1029/2011JD016630, 2012. 2811

Schlatter, T. W.: The local surface energy balance and subsurface temperature regime in Antarctica, J. Appl. Meteorol., 11, 1048–1062, doi:10.1175/1520-0450(1972)011<1048:TLSEBA>2.0.CO;2, 1972. 2810

Schuster, A.: Radiation through a foggy atmosphere, Astrophys. J., 21, 1–22, doi:10.1086/141186, 1905. 2810

Sergent, C., Chevrand, P., Lafeuille, J., and Marbouty, D.: Caractérisation optique de différents types de neige. Extinction de la lumière dans la neige, Le Journal de Physique Colloques, 48, C1-361–C1-367, doi:10.1051/jphyscol:1987150, 1987. 2805, 2822

TCD
7, 2801–2843, 2013

Sergent, C., Pougatch, E., Sudul, M., and Bourdelles, B.: Experimental investigation of optical snow properties, Ann. Glaciol., 17, 281–287, available at: http://adsabs.harvard.edu/abs/1993AnGla..17..281S, 1993. 2816

Sergent, C., Leroux, C., Pougatch, E., and Guirado, F.: Hemispherical-directional reflectance measurements of natural snows in the 0.9–1.45 µm spectral range: comparison with adding-doubling modelling, Ann. Glaciol., 26, 59–63, available at: http://adsabs.harvard.edu/abs/1998AnGla..26...59S, 1998. 2804, 2820

Shettle, E. P. and Weinman, J. A.: The transfer of solar irradiance through inhomogeneous turbid atmospheres evaluated by Eddington's approximation, J. Atmos. Sci., 27, 1048–1055, doi:10.1175/1520-0469(1970)027<1048:TTOSIT>2.0.CO;2, 1970. 2811

Stamnes, K., Tsay, S.-C., Wiscombe, W., and Jayaweera, K.: Numerically stable algorithm for discrete-ordinate-method radiative transfer in multiple scattering and emitting layered media, Appl. Optics, 27, 2502–2509, doi:10.1364/AO.27.002502, 1988. 2813, 2823

Takano, Y. and Liou, K.-N.: Solar radiative transfer in cirrus clouds. Part I: Single-scattering and optical properties of hexagonal ice crystals, J. Atmos. Sci., 46, 3–19, doi:10.1175/1520-0469(1989)046<0003:SRTICC>2.0.CO;2, 1989. 2813

Toon, O. B., McKay, C. P., Ackerman, T. P., and Santhanam, K.: Rapid calculation of radiative heating rates and photodissociation rates in inhomogeneous multiple scattering atmospheres, J. Geophys. Res., 94, 16287–16301, doi:10.1029/JD094iD13p16287, 1989. 2811

van den Broeke, M., Smeets, P., Ettema, J., van der Veen, C., van de Wal, R., and Oerlemans, J.: Partitioning of melt energy and meltwater fluxes in the ablation zone of the west Greenland ice sheet, The Cryosphere, 2, 179–189, doi:10.5194/tc-2-179-2008, 2008. 2804

Vionnet, V., Brun, E., Morin, S., Boone, A., Faroux, S., Le Moigne, P., Martin, E., and Willemet, J.-M.: The detailed snowpack scheme Crocus and its implementation in SURFEX v7.2, Geosci. Model Dev., 5, 773–791, doi:10.5194/gmd-5-773-2012, 2012. 2804

Vouk, V.: Projected area of convex bodies, Nature, 162, 330–331, doi:10.1038/162330a0, 1948. 2809

Waliser, D., Kim, J., Xue, Y., Chao, Y., Eldering, A., Fovell, R., Hall, A., Li, Q., Liou, K. N., McWilliams, J., Kapnick, S., Vasic, R., Sale, F., and Yu, Y.: Simulating cold season snowpack: impacts of snow albedo and multi-layer snow physics, Climatic Change, 109, 95–117, doi:10.1007/s10584-011-0312-5, 2011. 2803

Warren, S. G.: Optical properties of snow, Rev. Geophys., 20, 67–89, doi:10.1029/RG020i001p00067, 1982. 2803, 2804, 2807, 2824

TCD
7, 2801–2843, 2013

Warren, S. G.: Impurities in snow: effects on albedo and snowmelt, Ann. Glaciol., 5, 177–179, 1984. 2816

Warren, S. G. and Brandt, R. E.: Optical constants of ice from the ultraviolet to the microwave: a revised compilation, J. Geophys. Res., 113, D14220, doi:10.1029/2007JD009744, 2008. 2806, 2807

Warren, S. G. and Wiscombe, W. J.: A model for the spectral albedo of snow. II: Snow containing atmospheric aerosols, J. Atmos. Sci., 37, 2734–2745, doi:10.1175/1520-0469(1980)037<2734:AMFTSA>2.0.CO;2, 1980. 2811, 2812, 2816

Warren, S. G., Brandt, R. E., and Grenfell, T. C.: Visible and near-ultraviolet absorption spectrum of ice from transmission of solar radiation into snow, Appl. Optics, 45, 5320–5334, doi:10.1364/AO.45.005320, 2006. 2820

Wiscombe, W. J.: Improved Mie scattering algorithms, Appl. Optics, 19, 1505–1509, doi:10.1364/AO.19.001505, 1980. 2813, 2823

Wiscombe, W. J. and Warren, S. G.: A model for the spectral albedo of snow. I: Pure snow, J. Atmos. Sci., 37, 2712–2733, doi:10.1175/1520-0469(1980)037<2712:AMFTSA>2.0.CO;2, 1980. 2804, 2806, 2808, 2810, 2824

Wiscombe, W. T.: The Delta-Eddington Approximation for a Vertically Inhomogeneous Atmosphere, Tech. rep., available at: http://adsabs.harvard.edu/abs/1977deav.rept.....W, 1977. 2810, 2811

Xie, Y., Yang, P., Gao, B.-C., Kattawar, G. W., and Mishchenko, M. I.: Effect of ice crystal shape and effective size on snow bidirectional reflectance, J. Quant. Spectrosc. Ra., 100, 457–469, doi:10.1016/j.jqsrt.2005.11.056, 2006. 2813

Zatko, M. C., Grenfell, T. C., Alexander, B., Doherty, S. J., Thomas, J. L., and Yang, X.: The influence of snow grain size and impurities on the vertical profiles of actinic flux and associated NO_x emissions on the Antarctic and Greenland ice sheets, Atmos. Chem. Phys., 13, 3547–3567, doi:10.5194/acp-13-3547-2013, 2013. 2804, 2820

Zege, E., Katsev, I., Malinka, A., Prikhach, A., and Polonsky, I.: New algorithm to retrieve the effective snow grain size and pollution amount from satellite data, Ann. Glaciol., 49, 139–144, doi:10.3189/172756408787815004, 2008. 2804, 2807, 2809

TCD
7, 2801–2843, 2013

Table 1. Values of B and g^{G} for various geometric shapes, calculated using ray tracing methods. Values for spheroids, hexagonal plates and fractals are from Kokhanovsky and Macke (1997). The values for the other shapes were obtained with SnowRat (Picard et al., 2009). For hexagonal plates, cuboids and cylinders, the aspect ratio is the ratio of the height to, the length of the hexagonal side, the length of the square side and the radius of the circle, respectively. For spheroids, it is the ratio of the largest semiaxis to the shortest one.

Shape	Aspect ratio	g^{G}	B	Shape	Aspect ratio	g^{G}	B
Sphere	1	0.79	1.25	Fractals	–	0.50	1.84
Spheroid	0.5	0.63	2.09	Cube	1	0.54	1.56
Spheroid	0.7	0.69	1.60	Cuboid	2	0.59	1.58
Spheroid	1.5	0.70	1.36	Cuboid	4	0.66	1.60
Spheroid	2	0.71	1.43	Cylinder	0.25	0.80	1.41
Hexagonal plate	0.4	0.72	1.80	Cylinder	0.5	0.70	1.42
Hexagonal plate	1	0.57	1.60	Cylinder	1	0.63	1.44
Hexagonal plate	2	0.52	1.60	Cylinder	2	0.69	1.46
Hexagonal plate	4	0.59	1.80	Cylinder	4	0.77	1.48

TCD
7, 2801–2843, 2013

Table 2. Summary of the measurements collected at Dome C and in the Alps. DC: Dome C, CP: Col de Porte, LR: Lacs Robert, LP: Lac Poursollet. λ_1 and λ_2 are the specific wavelengths used in the algorithm described in Sect. 4.1. The retrieved values of B and BC are given.

Site	Date	Snow type	Type of extinction data	Instrument used to measure $\alpha(z)$	λ_1/λ_2 (nm)	B	BC (ng g^{-1})
DC1	Jan 2011	Hard Windpack	$\ell(\lambda)$	POSSSUM	500/700	1.9	8
DC2	Jan 2011	Depth Hoar	$\ell(\lambda)$	POSSSUM	500/700	2.0	3
CP1	24 Feb 2012	Rounded/facetted grains	$I(z,\lambda)$	ASSSAP	600/780	1.8	85
CP2	29 Feb 2012	Rounded/facetted grains	$I(z,\lambda)$	ASSSAP	600/780	1.9	15
CP3	9 Mar 2012	Fresh snow	$I(z,\lambda)$	DUFISSS	600/780	0.8	12
LR	13 Mar 2012	Fine/facetted grains	$I(z,\lambda)$	DUFISSS	600/780	1.6	12
LP	10 May 2012	Coarse grains	$I(z,\lambda)$	ASSSAP	600/780	1.6	50

TCD
7, 2801–2843, 2013

Table 3. Determination of B from data in the literature, using Eq. (12). λ_{k_e} and λ_{k_e} are in nm. R, T and E stand for reflectance, transmission and extinction, respectively and refer to the measurements performed in the corresponding study. The 5 largest values of B and the corresponding α values are bold.

Reference	Location	Meas. type	Snow type	ρ (kg m^{-3})	k_e (m^{-1})	λ_{k_e}	α	λ_α	B
Grenfell and Maykut (1977)	Beaufort Sea	R/E	Dry snow	400	44	700	0.89	800	2.8
			Wet old snow	470	26	700	**0.68**	800	**4.7**
Beaglehole et al. (1998)	Antarctica	T	Fresh snow	130	50	800	**0.79**	800	**9.9**
			not specified	340	46	800	**0.80**	800	**3.3**
			Drift snow	320	34	800	0.87	800	1.6
			Drift snow	360	44	800	0.93	800	1.0
Perovich (2007)	Hanover	R/T	Rounded grains	120	33	900	0.85	900	1.7
			Rounded grains	200	25	900	0.72	900	1.6
			Columns	143	26	850	0.86	850	2.3
			Wet snow	373	43	850	**0.70**	850	**3.5**
France et al. (2011a)	Svalbard	R/E	Old windpack	400	18	700	0.925	700	1.5
France et al. (2011b)	Dome C	R/E	Soft windpack	300	33	700	0.962	700	1.9
			Hard windpack	380	29	700	0.945	700	1.9
			Depth hoar	280	23	700	0.947	700	2.0
France et al. (2012)	Alaska	R/E	Inland snow	300	9	700	0.91	700	1.2
			Hard snowpack	380	30	700	**0.83**	700	**6.5**

TCD
7, 2801–2843, 2013

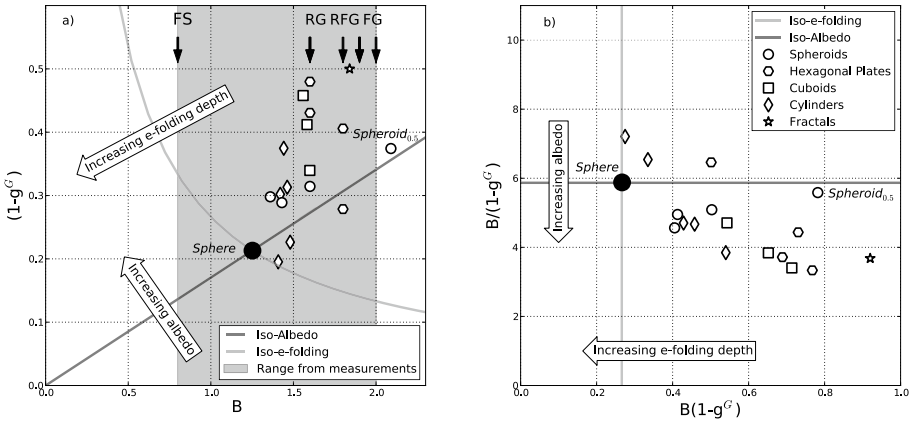

Fig. 1. (a) The shapes presented in Table 1 are displayed in a B,$(1-g^{\mathrm{G}})$ diagram. The thin arrows indicate the values of B retrieved from field measurements (Sect. 4). FS: Fresh Snow, RG: Rounded Grains, RFG: Rounded/Facetted Grains, FG: Facetted Grains. **(b)** The same shapes are presented in a $B(1-g^{\mathrm{G}})$,$B/(1-g^{\mathrm{G}})$ diagram, to illustrate their characteristics in terms of extinction and albedo (see Eqs. 10 and 11).

TCD
7, 2801–2843, 2013

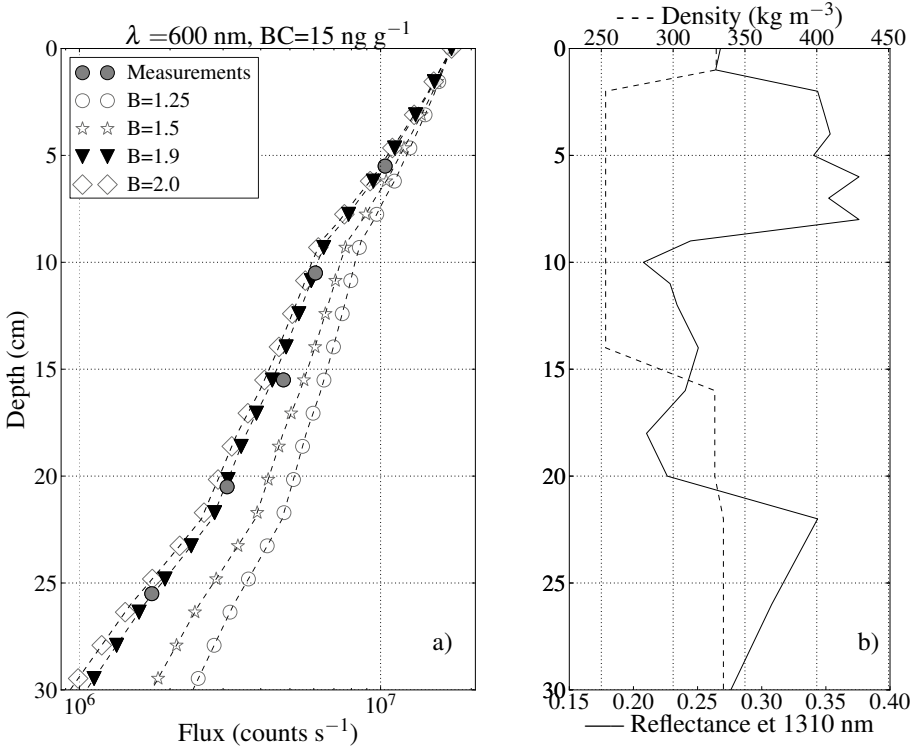

Fig. 2. Measurements conducted at Col de Porte (29 February 2012). **(a)** The measured intensity profile at λ = 600 nm is shown with the optimal modeled profile symbolized by dark inverted triangles. The other profiles have been calculated for various values of B and incident flux equal to the optimal F_0(600 nm). **(b)** Vertical profiles of density and reflectance at 1310 nm.

TCD
7, 2801–2843, 2013




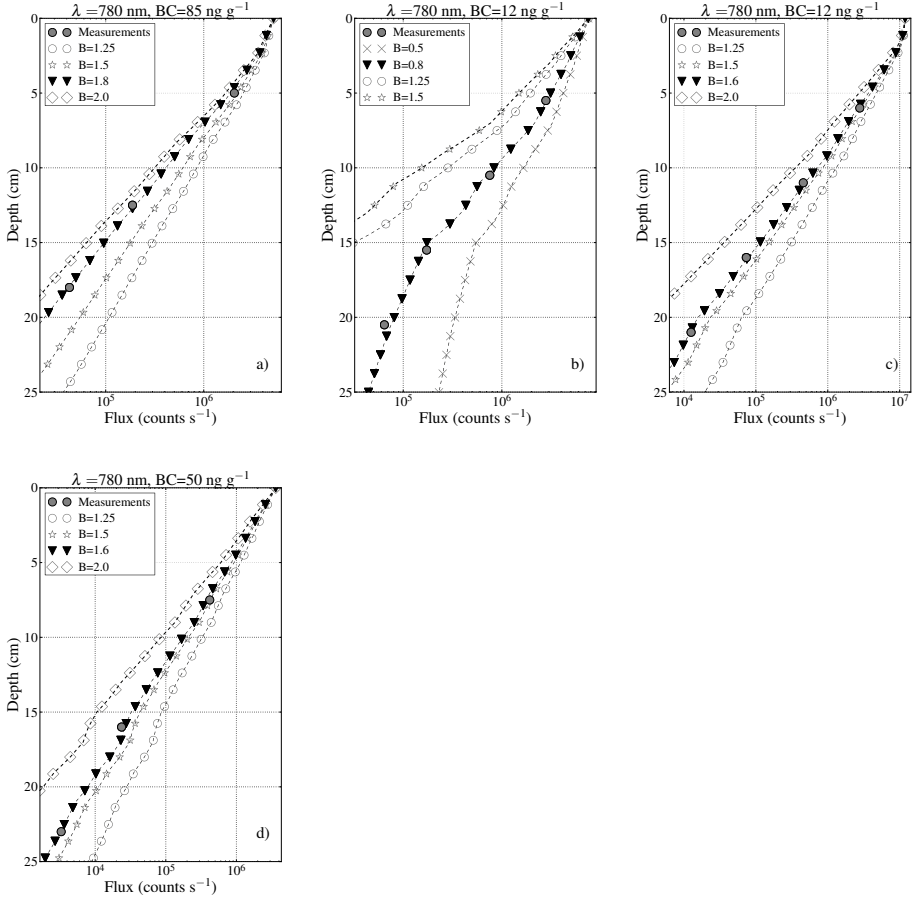

Fig. 3. Same as Fig. 2a for the 4 other Alpine sets of measurements. **(a)** Col de Porte (24 February 2012). **(b)** Col de Porte (9 March 2012). **(c)** Lacs Robert (13 March 2012). **(d)** Lacs Poursollet (10 May 2012).

TCD
7, 2801–2843, 2013

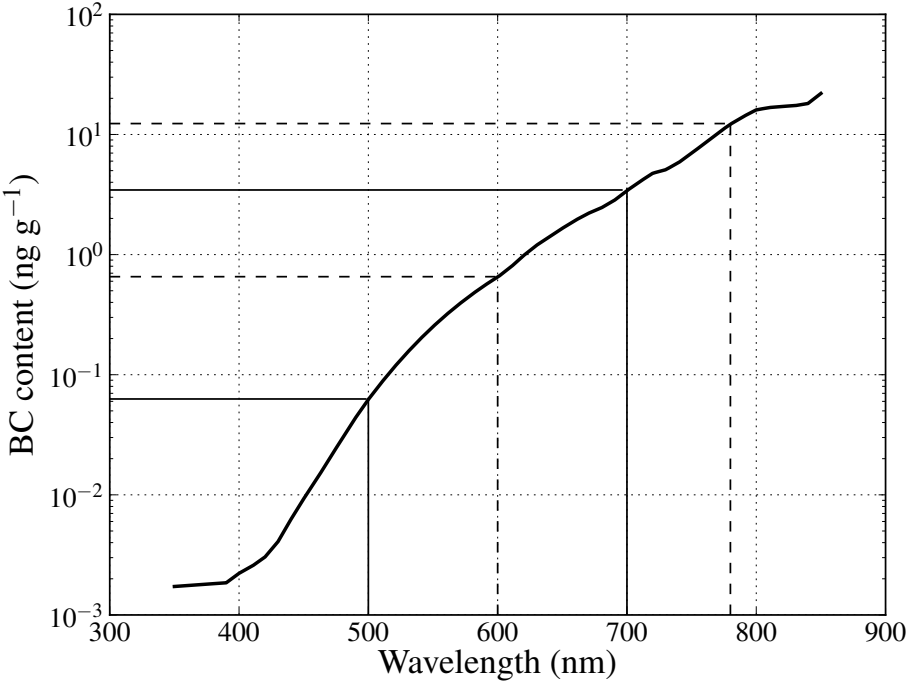

Fig. 4. BC content beyond which BC absorption represents more than 5 % of the snow absorption coefficient. The curve is deduced from Eq. (25). The dashed lines highlight the values at 600 nm and 780 nm and the continuous lines highlight the values at 500 nm and 700 nm.

TCD
7, 2801–2843, 2013

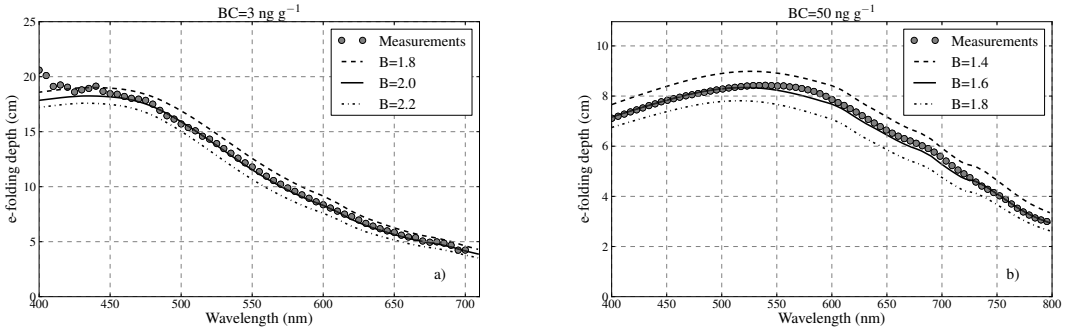

Fig. 5. (a) Spectral *e*-folding depth measured in the depth hoar layer at Dome C. Modeled spectral *e*-folding depths are also shown for different values of *B*. **(b)** Spectral *e*-folding depth measured between 7.5 cm and 23 cm at Lac Poursollet (10 May 2012) in a snowpack composed of coarse grains.

TCD
7, 2801–2843, 2013

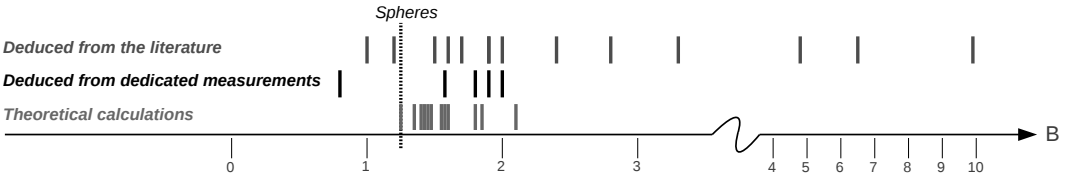

Fig. 6. Representation of all values of *B* determined from theoretical calculations, from measurements dedicated to this paper and from data in the literature.

TCD
7, 2801–2843, 2013